Journal of Biomolecular NMR, 9 (1997) 337–346

J-Bio NMR 436

Structural features of the metal binding site and dynamics of gallium putidaredoxin, a diamagnetic derivative of a $Cys_4Fe_2S_2$ ferredoxin

Sophia Kazanis[a] and Thomas C. Pochapsky[b,*]

[a]*Bioorganic Chemistry Program and* [b]*Department of Chemistry, Brandeis University, Waltham, MA 02254-9110, U.S.A.*

Received 13 December 1996
Accepted 19 February 1997

Keywords: Electron transfer; Putidaredoxin; Cytochrome P450; Metalloprotein; Gallium

Summary

The first reconstitution of an Fe_2S_2 ferredoxin with a diamagnetic prosthetic group was recently described [Kazanis et al. (1995) *J. Am. Chem. Soc.*, **117**, 6625–6626]. The replacement of the iron–sulfur cluster of the bacterial ferredoxin putidaredoxin (Pdx) by gallium (Ga^{3+}) renders the protein diamagnetic and permits the use of high-resolution NMR methods to identify resonances near the metal binding site. We now describe structural features of the metal binding site that are not observable by standard NMR methods in native Pdx due to paramagnetic line broadening. These results provide the first example of high-resolution NMR-derived structural data concerning the metal binding domain of an Fe_2S_2 ferredoxin, and the first structural information of any sort for the metal binding site of a ferredoxin from this class, which includes adrenodoxin, placental ferredoxin and terpredoxin. Assignments were obtained by applying multidimensional NMR methods to a series of selectively and nonselectively ^{15}N- and $^{13}C/^{15}N$-labeled GaPdx samples. For most experiments, a mutant of Pdx was used in which a nonligating Cys^{85} is replaced by serine. All of the major structural features that were identified in native Pdx are conserved in GaPdx. The overall protein dynamics is considerably faster in GaPdx than in the native protein, as reflected by amide proton exchange rates. The C-terminal residue, Trp^{106}, also exhibits considerable mobility, as indicated by $^{15}N\{^1H\}$ NOE and ^{15}N T_1 values of the C-terminal residue of the protein.

Introduction

The limiting factor in determining the applicability of NMR methods to paramagnetic proteins is the relaxation rates of the resonances of interest. In heme proteins, nuclear relaxation is often slow enough to permit the observation of nuclear Overhauser effects and J-couplings even for porphyrin ring resonances. However, for Fe_2S_2 ferredoxins, resonances tend to be quite broad in the vicinity of the metal cluster and nuclear relaxation very fast. Although the relaxation times of the methylene protons of cysteines ligating the metal center in reduced plant-type ferredoxins are long enough to permit the use of NOE techniques to identify ligation patterns (Dugad and La Mar, 1990), such methods have not been successfully applied to bacterial or mammalian Fe_2S_2 ferredoxins (Skjeldal et al., 1990; Ratnaswamy and Pochapsky, 1993).

An obvious way of circumventing paramagnetic line broadening is to replace the paramagnetic center of a protein with a diamagnetic prosthetic group. Substitution of Zn^{2+} for iron in the heme of horse heart cytochrome c yields a protein with the same overall structure, axial ligands and redox partner binding interfaces as the native iron-containing cytochrome (Anni et al., 1995). This approach was also adopted for studies of a rubredoxin from *Pyrococcus furiosus* in which the single iron atom was replaced by Zn^{2+} (Blake et al., 1992a). Structural studies showed that this substitution does not alter the global fold of the rubredoxin, and sequential resonance assignments were obtained for residues in the metal binding site (Blake et al., 1992b). We recently described the reconstitution of putidaredoxin (Pdx), a $Cys_4Fe_2S_2$ ferredoxin from *Pseudomonas putida*, with Ga^{3+}, yielding a colorless diamagnetic protein containing a single gallium

*To whom correspondence should be addressed.
Supplementary Material: Complete ^1H, ^{13}C and ^{15}N assignments for GaPdx are available from the corresponding author.

atom in which the major structural features of the native protein are conserved (Kazanis et al., 1995). Pdx is the archetype of a class of ferredoxins which transfer electrons to monooxygenases in bacterial and mammalian systems (Lipscomb et al., 1976), and is as yet the only member of this class for which a structure has been described (Pochapsky et al., 1994a). Other members of this class include terpredoxin, linredoxin and adrenodoxin (Tanaka et al., 1973; Berg et al., 1976; Ullah et al., 1983). The model that we presented for the solution structure of oxidized (Fe^{3+}-Fe^{3+}) native Pdx was based on experimentally derived NOE and dihedral restraints in regions of the protein further than 8 Å from the metal center. Near the metal center, the structure was modeled from crystallographic structures of plant ferredoxins. The gallium-reconstituted form of Pdx, GaPdx, was discovered in the course of a search for folded diamagnetic derivatives of Pdx that could be used to obtain structural information near the metal center of Pdx by solution NMR methods. GaPdx contains a single gallium ion, as determined by high-resolution mass spectrometry. Extended X-ray absorption fine structure (EXAFS) data are consistent with ligation of the gallium by four cysteinyl sulfurs, with ligation somewhat distorted from tetrahedral towards square planar, as expected if the gallium were replacing the Fe_2S_2 cluster (Kazanis et al., 1995). We now present a structural and dynamic analysis of NMR data obtained using a variety of selectively and uniformly ^{15}N- and $^{13}C/^{15}N$-labeled GaPdx samples. Observed NOE patterns allow us to confirm that secondary structural elements and tertiary interactions similar to those in the native protein are conserved in GaPdx. We also describe non-sequential NOEs in the vicinity of the metal binding site, providing direct experimental data concerning critical structural features of this protein, the first such observations for any member of this class of ferredoxin.

Materials and Methods

Sample preparation

For many of the experiments described, a mutant of Pdx (C85S) was used in which a nonligating cysteine, Cys^{85}, is replaced by serine (Gerber et al., 1990). Wild-type Pdx does reconstitute with gallium salts, giving a product similar by NMR analysis to that obtained from the C85S mutant. However, some minor product, presumably formed by misligation of gallium, was observed in reconstitutions of the wild-type protein. The C85S mutant appears to give only a single product upon reconstitution, and so was particularly suited for the more costly isotopic labeling experiments. Uniformly labeled ^{15}N and $^{15}N/^{13}C$ samples of wild-type and C85S Pdx were overexpressed using the *E. coli* cell strain NCM533 (*lacI+*) transformed with the plasmid pKM536, which contains the wild-type Pdx gene (*camB*) under control of the *lac* promoter. A modified version of pKM536 that encodes the C85S mutant of Pdx was used to obtain expression of that mutant (Gerber et al., 1990). Cultures were grown on minimal M9 media containing either $^{15}NH_4Cl$ or both $^{15}NH_4Cl$ and U-^{13}C glycerol (Lyons et al., 1996). For the selectively labeled ^{15}N-alanine and ^{15}N-cysteine samples, the NCM533 strain was transformed with pKM536 and plated on an LB agar plate containing 200 μg/ml ampicillin and 50 μg/ml kanamycin and incubated overnight at 37 °C. A single colony taken from the plate was allowed to grow in 5 ml of LB until an $OD_{600} \sim 0.5$ was reached. This culture was diluted with 50 ml of LB and allowed to continue growing until an $OD_{600} \sim 0.5$ was reached. At this point, the cells were pelleted centrifugally and resuspended in 50 ml of M9 media containing $FeCl_3$, thiamin and trace amounts of B, Mn, Zn, Mo, Cu and Co salts. This culture was allowed to acclimate for 2 h at 37 °C before being inoculated into 1 l of M9 media. At an $OD_{600} = 0.5$, a 20 ml solution containing 100 mg of each amino acid (excluding proline) including 50 mg of the appropriate ^{15}N-labeled amino acid (Cambridge Isotope Laboratories, Andover, MA, U.S.A.) was added and expression was induced by the addition of isopropyl-β-D-thiogalactopyranoside (IPTG) to a final concentration of 0.5 mM. The cells were harvested after 12 h by centrifugation. Pdx samples were purified from cell extract and reconstituted with aqueous $GaCl_3$ as previously described (Kazanis et al., 1995; Lyons et al., 1996). The GaPdx sample was then diluted into the appropriate buffer and concentrated using centrifugal filtration. NMR samples were typically 1–2 mM GaPdx in 50 mM *d*-Tris-HCl (pH 7.4) in 10% D_2O/90% H_2O. Small amounts (<10 mM) of 2-hydroxyethanethiol were added as a preservative to the reconstituted GaPdx samples. Reported pH values are uncorrected for isotope effects.

NMR spectroscopy

All NMR experiments were recorded at 290 or 298 K on either a Bruker AMX-500 spectrometer equipped with a three-channel Acustar pulsed field gradient amplifier and an x,y,z-gradient triple-resonance inverse detection probe (Brandeis University), or on similarly equipped Bruker DRX-500 or DMX-600 spectrometers (Bruker Instruments, Billerica, MA, U.S.A.). The AMX-500 and DRX-500 spectrometers operate at 500.13, 50.68 and 125.76 MHz for ^1H, ^{15}N and ^{13}C, respectively. The DMX-600 operates at 600.13, 60.81 and 150.9 MHz for ^1H, ^{15}N and ^{13}C, respectively. All ^1H chemical shifts are referenced to external DSS using the water signal as internal reference. ^{15}N chemical shifts are reported relative to external liquid ammonia using the ^1H resonance of H_2O (Live et al., 1984) and ^{13}C chemical shifts are reported relative to the methyl resonance of external DSS (Bax and Subramanian, 1986). Quadrature detection in the indirect dimension was achieved for all experiments using either

hypercomplex or time-proportional phase incrementation (TPPI) data acquisition. Either GARP-1 (Shaka et al., 1985) or WALTZ-16 (Shaka et al., 1983) composite pulse decoupling schemes were used for broadband decoupling of heteronuclei during acquisition.

Homonuclear experiments

Two-dimensional (2D) homonuclear NOESY (Kumar et al., 1980), HOHAHA (Bax and Davis, 1985) and magic-angle-gradient DQF-COSY (Van Zijl et al., 1995) experiments were recorded at 500 MHz on the AMX-500 with spectral widths of 8064 Hz and 400–500 t_1 increments. A 7.5 kHz DIPSI-2 composite pulse spin lock (Shaka et al., 1988) was applied for a mixing time of 60 ms in the HOHAHA experiment. A mixing time of 75 ms was used for the NOESY experiment. Water suppression was achieved in the NOESY experiment using the WATERGATE sequence (Piotto et al., 1992). Selective square flip-back pulses, which return water magnetization to the +z axis, were also incorporated into the NOESY sequence (Lippens et al., 1995) in order to minimize saturation transfer from solvent.

^{15}N-separated experiments

For ^{15}N-separated experiments performed at 500 MHz (^{1}H), the ^{15}N carrier frequency was placed in the center of the amide nitrogen region (120 ppm), the ^{15}N spectral width was set to 2027 Hz and the ^{1}H spectral width to 8064 Hz. For ^{15}N-separated experiments performed at 600 MHz (^{1}H), the ^{15}N carrier frequency was placed at 120 ppm, the ^{15}N spectral width was set to 2003 Hz and the ^{1}H spectral width to 8012 Hz. Water suppression for all ^{15}N-selective experiments was achieved using a WATERGATE sequence (Piotto et al., 1992). A 2D 'flip-back' HSQC (Grzesiek and Bax, 1993) was recorded with 128 t_1 increments. A three-dimensional (3D) NOESY-HSQC experiment (Marion et al., 1989a) was recorded with a mixing time of 70 ms. A 3D TOCSY-HSQC (Marion et al., 1989b) was recorded with a 7.5 kHz spin-locking field applied during a 60 ms isotropic mixing time. The ^{1}H spin-locking field was generated using a DIPSI-2 sequence. Eight FIDs were recorded per data point with 128 real points collected in t_1 (^{1}H), 64 real points in t_2 (^{15}N) and 512 complex points in t_3 (^{1}H) for both the TOCSY-HSQC and NOESY-HSQC experiments. $^3J_{NH\text{-}C^{\alpha}H}$ coupling constants were measured using a series of J-modulated [^{15}N, ^{1}H]-COSY experiments (Neri et al., 1990). Delay times of 20, 30, 40, 50, 60, 70, 80, 90, 110 and 120 ms were used for coupling evolution in these experiments, with 64 FIDs recorded for each of 128 t_1 increments.

^{15}N, ^{13}C-separated experiments

Constant-time HNCA and HN(CO)CA experiments were recorded on the AMX-500 spectrometer (Bax and Pochapsky, 1992; Grzesiek and Bax, 1992). Off-resonance carbonyl decoupling was accomplished for these experiments using phase-modulated shaped pulses. For both experiments, the ^{15}N carrier frequency was set to 120 ppm, the ^{13}C carrier frequency was set to 60.4 ppm and the ^{1}H carrier frequency was set at the water resonance with the corresponding spectral widths 2027 Hz (^{15}N), 3180 Hz (^{13}C) and 8064 Hz (^{1}H). Thirty-two FIDs were recorded per data point with 64 real points collected in t_1 (^{15}N), 90 real points in t_2 (^{13}C) and 512 complex points in t_3 (^{1}H). A sensitivity-enhanced constant-time HNCO experiment was also recorded (Kay et al., 1994). Decoupling of the C^{α} from carbonyl carbon resonances was achieved using a 2.5 ms SEDUCE shaped pulse (McCoy and Mueller, 1992a,b). Sixteen FIDs were recorded per data point with 64 real points collected in t_1 (^{15}N), 80 real points in t_2 (^{13}C) and 512 complex points in t_3 (^{1}H).

^{13}C-separated experiments

Three different 2D ^{13}C-separated constant-time HSQC experiments (Vuister and Bax, 1992) were performed on the AMX-500 spectrometer. The first two experiments were selective for aliphatic resonances with the ^{13}C carrier frequency set to 40.9 ppm and a ^{13}C spectral width of 8440 Hz. A constant-time delay of either 14.7 ms ($1/J_{CC}$) or 29.4 ms ($2/J_{CC}$) was used in the sequence. The experiment containing the shorter delay gives rise to correlation peaks, the sign of which depends on the CH multiplicity, but, because of time constraints, limits the resolution in the ^{13}C dimension (450 t_1 values). The longer delay yields correlations all of the same sign, but allows for higher resolution in the ^{13}C dimension (900 t_1 values). In both experiments, 1024 complex points were collected in t_2 (^{1}H), and a ^{1}H spectral width of 6024 Hz was used. The third experiment was selective for aromatic resonances with the ^{13}C carrier frequency set to 135.5 ppm and a ^{13}C spectral width of 7162 Hz. Sixteen FIDs were accumulated at each of 400 t_1 (^{13}C) real points, with 1024 complex points in t_2 (^{1}H). A standard incremented-time HSQC was also performed with these parameters in which direct ^{13}C-^{13}C coupling was permitted to evolve in the t_1 dimension in order to aid in the assignment of aromatic spin systems.

A modified 3D HCCH-TOCSY experiment (Bax et al., 1990) was recorded, using a DIPSI-3 spin-locking sequence (Shaka et al., 1988) and a mixing time of 15.9 ms. The ^{1}H carrier frequency was initially set in the middle of the aliphatic region (2.70 ppm) with a spectral width of 3440 Hz and then switched to the water resonance for two consecutive spin-locking cycles in order to attenuate the water signal. The ^{13}C carrier frequency was centered at 40.9 ppm with a spectral width of 8440 Hz. Thirty-two FIDs were accumulated at each of 110 increments in t_1 (^{1}H) and 56 increments in t_2 (^{13}C). For each FID (^{1}H) 1024 complex points in t_3 were acquired. A modified 3D ^{13}C-edited HSQC-NOESY experiment (Majumdar and Zuiderweg, 1993) was also recorded using an NOE mixing

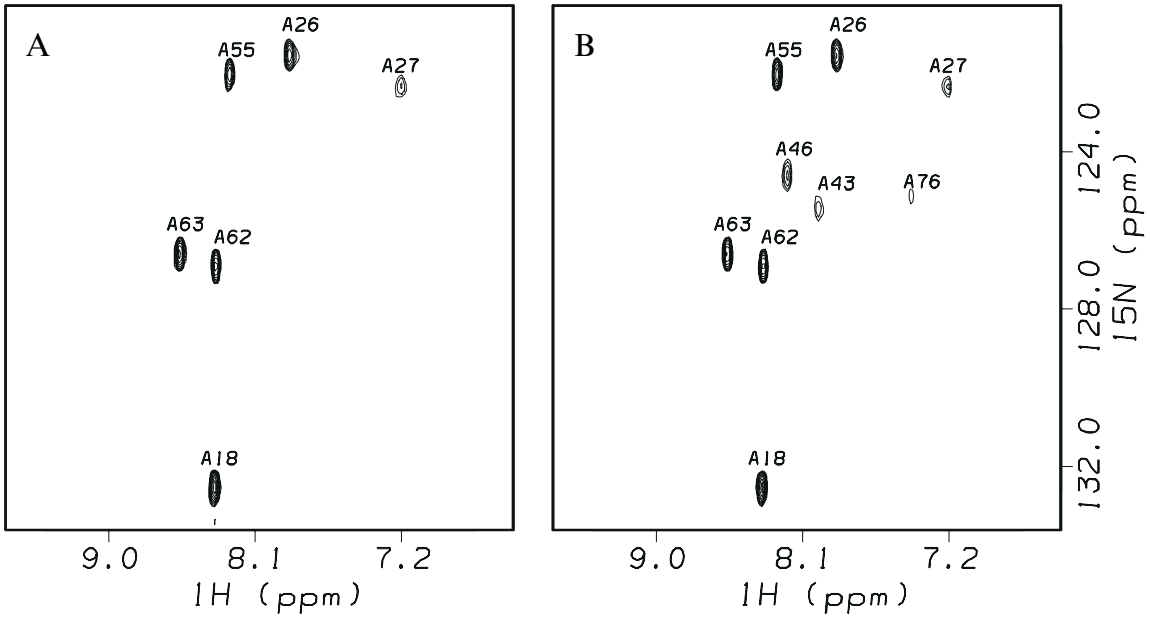

Fig. 1. ^{1}H-^{15}N HSQC of GaPdx selectively labeled with ^{15}N-alanine in 90%/10% H_2O/D_2O containing 50 mM *d*-Tris-HCl (pH 7.4, 298 K) obtained at 500 MHz (^{1}H). (A) Spectrum obtained using presaturation for solvent suppression. (B) Spectrum obtained using WATERGATE solvent suppression. Numbers correspond to the Ala residue to which N-H correlation is assigned. See the text for a complete description.

time of 75 ms. The ^{1}H carrier frequency was switched from the water resonance to the middle of the aliphatic region during t_1 evolution, allowing for increased resolution in the indirectly detected ^{1}H dimension. The ^{13}C carrier frequency was set to 43.3 ppm with a spectral width of 8960 Hz. Thirty-two FIDs were accumulated at each of 64 increments in t_1 (^{13}C) and 128 increments in t_2 (^{1}H). Each FID was acquired with 1024 complex points in t_3 (^{1}H).

H/D amide proton exchange, $^{15}N\{^{1}H\}$ NOE and ^{15}N T_1 relaxation experiments

Samples of uniformly ^{15}N-labeled GaPdx (1–2 mM) initially in 10% D_2O/90% H_2O buffered with 50 mM *d*-Tris-HCl (pH 7.4) and 10 mM 2-hydroxyethanethiol were exchanged into 100% D_2O buffered with 50 mM *d*-Tris-HCl, pH (apparent) 7.4, with 10 mM 2-hydroxyethanethiol using a pre-equilibrated spin column packed with size exclusion gel (Biorad P-2). After exchange, the samples were allowed to equilibrate in the spectrometer for a short time at 290 K. A series of 2D ^{1}H-^{15}N HSQC experiments were then continuously recorded for the first 7–8 h followed by one data set per hour for the next 12 h. All experiments were processed identically and cross-peak volumes were measured using the volume integration routine in FELIX.

^{15}N T_1 relaxation and $^{15}N\{^{1}H\}$ NOE measurements were performed using the modified ^{1}H-^{15}N HSQC experiments described by Kay et al. (1989) into which the WATERGATE sequence and flip-back pulses were incorporated appropriately for water suppression. ^{15}N T_1 values were calculated by fitting peak volumes obtained in a series of experiments incorporating relaxation delays of 50, 200, 350, 500, 650, 800 and 900 ms to a single exponential decay curve. $^{15}N\{^{1}H\}$ NOE values were calculated as the fractional enhancements of peak volumes obtained after 3 s of broadband ^{1}H presaturation (obtained by a series of 120° pulses spaced at 20 ms intervals) to those obtained without broadband saturation of ^{1}H.

Data processing

NMR spectra were processed and analyzed on a Silicon Graphics Indigo II workstation using FELIX version 95.0 (Biosym Technologies, San Diego, CA, U.S.A.). Processing of the data involved multiplication of the acquired FIDs by a Gaussian function in the directly detected dimension and a shifted $(\sin)^2$ function in indirectly detected dimensions. Prior to Fourier transformation, interferograms in the indirectly detected dimensions were zero filled at least twice in order to enhance apparent resolution. When appropriate, the low-frequency component of FIDs due to the water signal was removed by multiplication with a convolution difference function. A linear prediction of 10% additional points in the indirectly acquired dimensions was applied to reduce signal loss from window function multiplication (Olejniczak and Eaton, 1990).

Results

^{1}H, ^{15}N and ^{13}C resonance assignments

The assignment of the sequential backbone ^{1}H and ^{15}N resonances of GaPdx was greatly facilitated by the availability of the ^{1}H and ^{15}N resonance assignments of native

oxidized Pdx (Ye et al., 1992; Lyons et al., 1996). In order to assign resonances that are unobservable in native Pdx, particularly those in the metal binding loop (Val^{36}–His^{49}), we focused on identifying particular amino acid types using selective labeling methods. A set of selectively ^{15}N-labeled GaPdx samples was generated, including ^{15}N-Ala-, ^{15}N-Cys- and ^{15}N-Gly-GaPdx. In the case of the ^{15}N-Ala- and ^{15}N-Cys-labeled samples, no scrambling of label was observed, although a smaller than expected signal intensity of the ^{15}N-Cys-labeled sample indicated that the label was being diluted. The ^{15}N-Gly-label was observed to scramble to serines and cysteines, although the distinctive shifts of the glycine nitrogen resonances, combined with the data obtained from the ^{15}N-Cys-labeled sample and previous sequential assignments, were sufficient to unambiguously identify the glycine and serine resonances in ^{1}H-^{15}N HSQC spectra.

It became apparent at this point that presaturation as a method of water suppression was for the most part unsuited to the NMR analysis of GaPdx. ^{1}H-^{15}N HSQC spectra of selectively labeled samples obtained using presaturation for water suppression did not show all of the expected correlations. However, when nonsaturating water suppression methods were used (sequences incorporating water flip-back pulses and WATERGATE antiselective pulse suppression schemes, vide supra), all of the expected resonances were observed. This is best illustrated with the ^{15}N-Ala-labeled sample. As seen in Fig. 1, correlations for Ala^{43}, Ala^{46} and Ala^{76} are missing in spectra obtained with presaturation, but are clearly observed when WATERGATE is used. On the basis of this observation, we concluded that many of the amide protons in GaPdx undergo relatively rapid exchange with water, particularly in the metal binding site, and that saturation transfer posed a serious problem. These problems were particularly acute in $^{1}H,^{1}H$ NOESY spectra. NOESY spectra obtained with presaturation gave uniformly disappointing results despite variations in temperature and mixing times. However, the use of a $^{1}H,^{1}H$ NOESY sequence incorporating flip-back pulses and WATERGATE water suppression (Lippens et al., 1995) resulted in a large improvement in signal to noise, with recovery of many

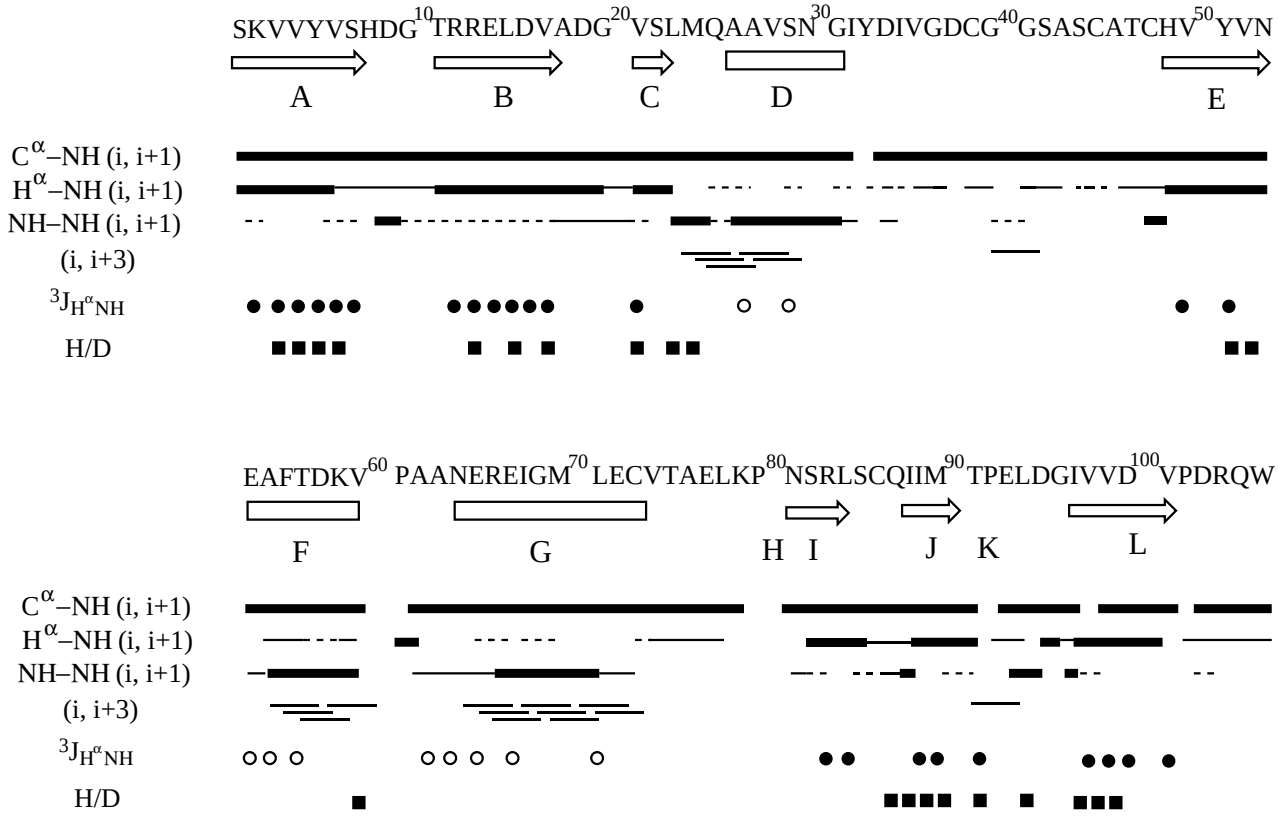

Fig. 2. Schematic of sequential connectivities and secondary structural elements of GaPdx. Secondary structural elements are listed immediately below the sequence. Arrows correspond to β-strands, rectangles to α-helices. Boldface lettering below the secondary structure markers corresponds to structural elements identified in Fig. 6. C^{α}-NH (i,i+1) correlations indicate identified scalar correlations. Sequential NOE connectivities are indicated as H^{α}-NH (i,i+1), NH-NH (i,i+1) and (i,i+3), which represent either H^{α}-NH or H^{α}-H^{β} (i,i+3) connectivities. Strong NOEs are represented by thick lines, medium NOEs by thin solid lines, and weak NOEs by dashed lines. $^{3}J_{H^{\alpha}\text{-NH}}$ are the three-bond (vicinal) couplings between NH and $C^{\alpha}H$ protons. Open circles represent vicinal coupling constants ≤5 Hz. Filled circles represent vicinal coupling constants that are ≥9 Hz. Amide protons which are protected from fast exchange in H/D exchange experiments, i.e. that are observed in the first ^{15}N-^{1}H HSQC after exchange into D_2O, are marked with filled squares.

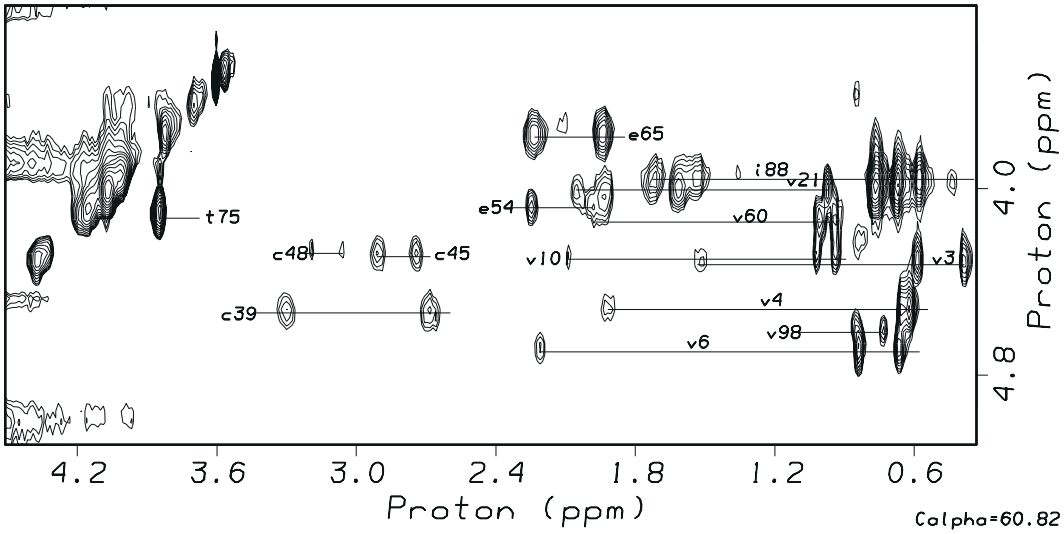

Fig. 3. ^{13}C plane from the 3D HCCH-TOCSY spectrum of GaPdx (90%/10% H_2O/D_2O, 50 mM *d*-Tris-HCl, pH 7.4, 298 K) obtained at 500 MHz (^1H). The plane (^{13}C shift = 60.8 ppm) corresponds approximately to the C^α chemical shift of three of the four cysteinyl ligands of the metal center, Cys^{39}, Cys^{45} and Cys^{48}. $C^\alpha H$-$C^\beta H$ correlations for these residues, as well as the side-chain correlations of various other residues, are marked.

correlations not observed in NOESY spectra obtained with presaturation.

Through-bond heteronuclear correlations were obtained via the HNCA and HN(CO)CA experiments using uniformly ^{13}C,^{15}N-labeled samples. The HNCA experiment correlates the NH proton to its own α-carbon. For most NH resonances in GaPdx, a remote peak was observed in the HNCA spectrum which correlated the NH proton to the α-carbon of the previous residue, as well. These connectivities could then be confirmed using the HN(CO)CA experiment, which exclusively correlates the NH proton to the α-carbon of the previous residue. Sequential connectivities are summarized in Fig. 2.

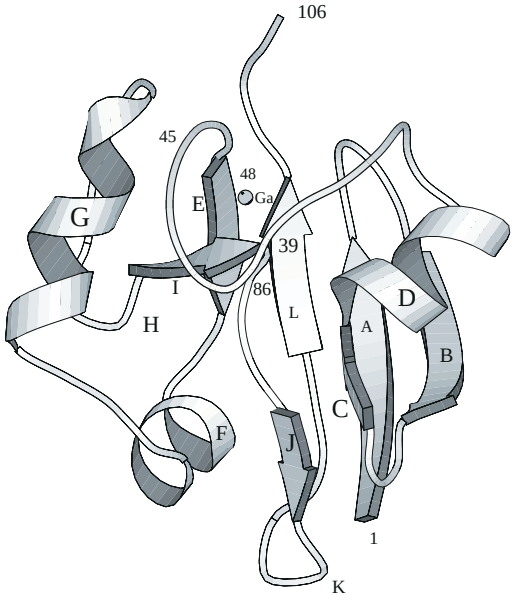

Fig. 4. Global fold of GaPdx with the secondary elements labeled as shown in Fig. 2. The structure was generated using a previously described simulated annealing protocol (Pochapsky et al., 1994a) incorporating new NOE restraints on the metal center as described in the text. Residues in elements are **A** (Ser^1–Ser^7), **B** (Arg^{12}–Val^{17}), **C** (Val^{21}–Ser^{22}), **D** (Leu^{23}–Asn^{30}), **E** (Val^{50}–Asn^{53}), **F** (Ala^{55}–Val^{60}), **G** (Asn^{64}–Val^{74}), **H** (Lys^{79}–Ser^{82}), **I** (Ser^{82}–Ser^{85}), **J** (Ile^{88}–Met^{90}), **K** (Thr^{91}–Leu^{94}), and **L** (Ile^{97}–Val^{101}). This figure was generated using MOLSCRIPT (Kraulis, 1991).

Side-chain ^{13}C resonances were then assigned using 3D HCCH-TOCSY and ^{13}C HSQC-NOESY data in conjunction with the ^1H-^{13}C CT-HSQC spectrum. The identification of side-chain resonances of the presumed cysteine ligands for the metal center was straightforward; the cysteine C^β-H correlations occur in a distinctive region of the ^1H-^{13}C CT-HSQC spectrum and, combined with HCCH-TOCSY data, the cysteine $C^\beta H_2$ resonances could be connected to the protein backbone and identified sequentially (Fig. 3).

Assignments for aromatic side-chain C-H correlations were made using a combination of NOESY and ^1H-^{13}C CT-HSQC data. The ^1H chemical shifts of aromatic protons could be assigned from homonuclear spectra for all three tyrosines, as well as for the unique phenylalanine and tryptophan residues of Pdx. Assignment of the protonated aromatic ^{13}C resonances for those residues by direct correlation was straightforward in HSQC spectra. Only partial assignments of the two histidine imidazoles (His^8 and His^{49}) could be made, presumably because exchange between protonated and unprotonated forms is significant at the pH required for this work (~7).

Secondary structural elements, global fold and local dynamics of GaPdx

Analysis of NOE data obtained from 2D and 3D experiments confirms that the secondary structural features

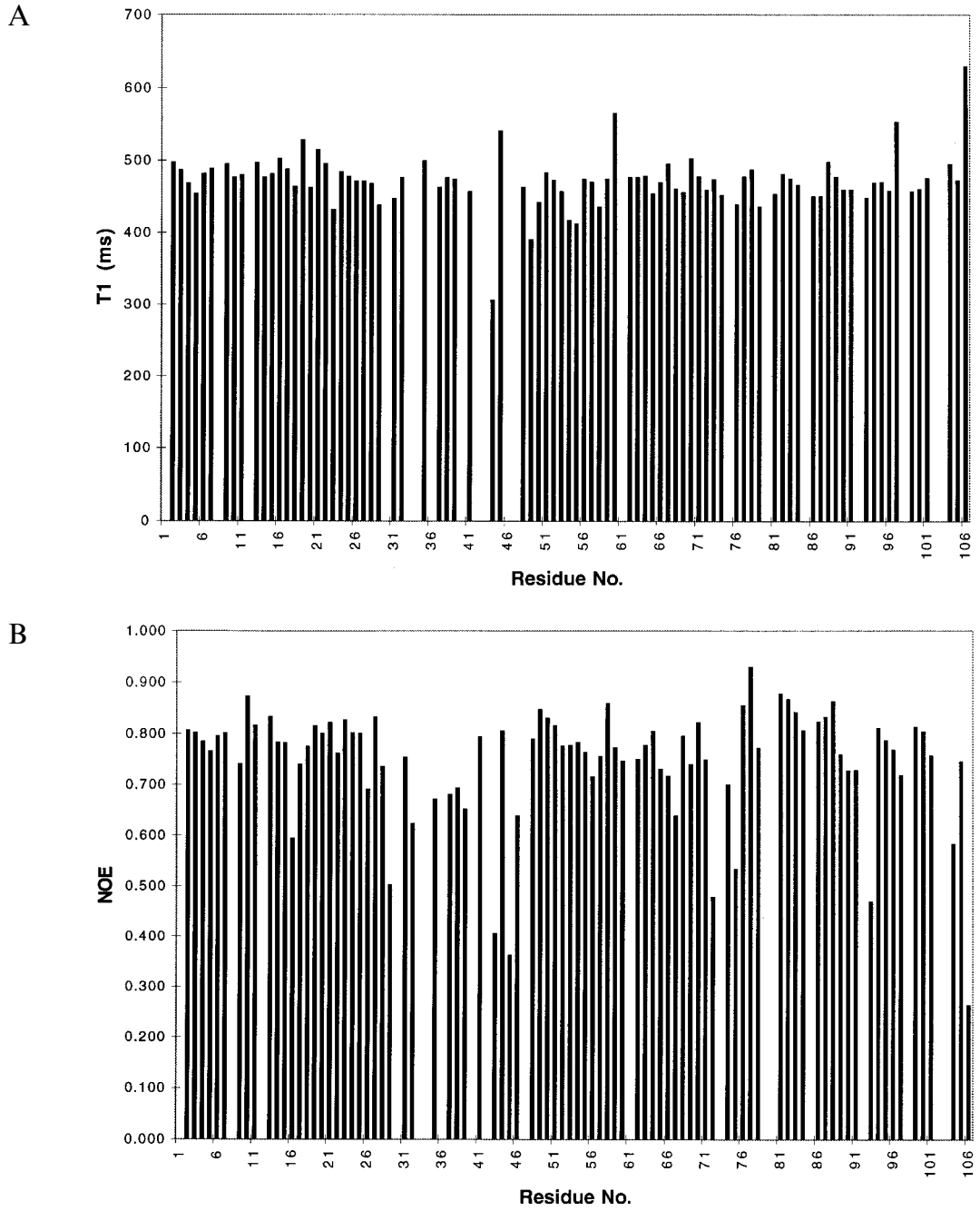

Fig. 5. Observed ^{15}N T_1 relaxation times (top) and steady-state $^{15}N\{^1H\}$ NOEs (bottom) in GaPdx as a function of sequence position measured at 298 K. From a comparison of data sets, the error in T_1 measurements is estimated to be ±10 ms, and NOE measurements are estimated to be accurate within 5% of the reported values.

of native Pdx are conserved in GaPdx in regions where comparison is possible. A five-stranded β-sheet, previously identified in the native protein, has also been identified in GaPdx (Fig. 4). This extensive sheet provides a scaffold for other structural features of the molecule, with side chains from strands A, B, E and L contributing to the hydrophobic core of the protein. This sheet appears to be essentially isostructural in GaPdx and native protein, and amide proton exchange measurements show that the slowest exchanging protons in the GaPdx β-sheet correspond to those which exchange most slowly in the native protein. The absence of paramagnetic broadening in GaPdx allowed the assignment of Leu[84] and Ser(Cys)[85], both of which appear to be in extended conformation and show strong $C^{\alpha}H$-NH (i,i+1) NOEs from the previous residue. Both also exhibit the downfield NH shifts typical of residues in β-sheets, and therefore represent the extension of strand I from that described previously for the native protein by two residues (Ye et al., 1992). On the adjacent antiparallel strand E, the NH of Val[50] detects a

strong NOE from the $C^{\alpha}H$ of His^{49}. However, a number of data indicate that His^{49} does not form an extension of strand E. First, the NH shift of His^{49} is further upfield (7.25 ppm) than is typical for residues in β-sheets. Second, a strong NH-NH NOE is observed between Cys^{48} and His^{49}, which is not typical of extended conformations. If His^{49} did form part of strand E, it would be expected that a $C^{\alpha}H$-$C^{\alpha}H$ NOE between His^{49} and Leu^{84} would be observed, a correlation that could not be unambiguously identified due to spectral overlap. However, a weak but unambiguous $C^{\alpha}H$-$C^{\alpha}H$ NOE is observed between Cys^{48} and Ser^{85}, which is inconsistent with a continuous regular β-sheet structure extending from the Tyr^{51}–Ser^{82} pairing. His^{49} therefore appears to form a 'bulge' in strand E which allows the Cys^{48} side chain to attain the orientation required to ligate the metal center.

Other secondary structural features of the native protein which are conserved in GaPdx include a smaller β-sheet, made up of short (two-residue) stretches of peptide, strands C and J, and two type I β-turns, H and K. Turn H forms one edge of the large β-sheet discussed above, while turn K begins immediately after strand J of the smaller β-sheet. A strong $C^{\alpha}H$-NH (i,i+1) NOE from Ile^{88} to Ile^{89}, the first residue in strand J, suggests that Ile^{88} is also in extended conformation. A strong NH-NH NOE from Gln^{87} to Ile^{88} indicates a break in the β-strand at this point.

Three α-helices, shown as D, F and G in Fig. 4, were identified in the native protein and are conserved in GaPdx. Helix D contains two residues, Met^{24} and Gln^{25}, for which many resonances could not be identified in native Pdx due to paramagnetic broadening. These residues are now completely assigned, and their positions within helix D confirmed. Met^{70} and Leu^{71} in helix G were also mostly unobservable in native protein but are clearly observed in GaPdx. A $C^{\alpha}H$-NH (i,i+3) NOE from Leu^{71} to Val^{74}, not detected in native Pdx, confirms that Val^{74} takes part in the formation of helix G.

Where comparisons can be made, the tertiary structure of native Pdx appears to be conserved in GaPdx. All tertiary contacts identified in the hydrophobic core of native Pdx are unperturbed by gallium reconstitution, and structural markers such as ring current shifts from aromatic residues to particular resonances are essentially identical in native and GaPdx.

Besides the hydrophobic core, a second compact region was identified in the structure of native Pdx. Termed the C-terminal cluster, this region is formed by interaction between side chains from the loop between helix G and turn H (Val^{74}–Thr^{75}–Ala^{76}–Lys^{77}–Leu^{78}), side chains from β-strands E (His^{49} and Tyr^{51}) and I (Ser^{82}), as well as the C-terminal residues Pro^{102}–Trp^{106} (Pochapsky et al., 1994b). Unlike the hydrophobic core, the C-terminal cluster appears to be held together by a combination of hydrophobic and hydrogen-bonding interactions (Pochapsky et al., 1994a,b). The C-terminal cluster is the most responsive region of Pdx to changes in charge at the metal center, with redox-dependent changes in chemical shifts and amide proton exchange rates observed in the native protein (Pochapsky et al., 1994b; Lyons et al., 1996). The C-terminal cluster of Pdx also exhibits the largest differences between the native protein and GaPdx. Exchange of the Ser^{82} OH and His^{49} $N_{\delta 1}H$ protons with solvent (slow enough in native Pdx for these resonances to be detected discretely) becomes fast on the chemical shift time scale in GaPdx. The NH resonances of Thr^{75}, Ala^{76}, Leu^{78} and Lys^{79} are broadened compared to the corresponding resonances in native Pdx, indicating that some dynamic process on the time scale of proton T_2 relaxation is occurring in portions of this loop. The observation of $^{15}N\{^1H\}$ NOEs greater than the theoretical maximum (+0.82) can be attributed to chemical exchange between water and the amide protons (Clore et al., 1990; Powers et al., 1992). Several $^{15}N\{^1H\}$ NOEs greater than +0.82 are observed for residues in the C-terminal cluster (Thr^{75}, Ala^{76}, Ser^{82}, Arg^{83}), providing evidence that chemical exchange is probably responsible for the NH line broadening (Fig. 5). Although the structural markers of the C-terminal cluster remain (chemical shifts are relatively unperturbed, and most of the NOEs that were detected in the native protein are still observed), NOEs observed in native Pdx between the indole ring resonances of the C-terminal residue Trp^{106} and the methyls of Val^{74} are not seen in GaPdx, indicating that the Trp^{106} side chain is much less constrained in GaPdx than in the native protein. $^{15}N\{^1H\}$ NOE and ^{15}N T_1 measurements confirm that the C-terminal residue of GaPdx (Trp^{106}) is more dynamic than the rest of the protein (Fig. 5). The Trp^{106} indole ring resonances exhibit considerable differences in chemical shifts and NOEs between oxidized and reduced Pdx, with the oxidized protein showing evidence of greater conformational freedom for the C-terminal residue (Pochapsky et al., 1994b; Lyons et al., 1996), and these perturbations are even larger when the metal cluster is replaced with a nonnative prosthetic group.

Constraints on the metal binding site of GaPdx

The Fe_2S_2 cluster of Pdx has been shown to be ligated by the side chains of Cys^{39}, Cys^{45}, Cys^{48} and Cys^{86} (Gerber et al., 1990), and it seemed likely that this was also the case for GaPdx. As noted above, both wild-type and C85S Pdx (which is expressed as a fully folded holoprotein spectroscopically and structurally indistinguishable from wild-type Pdx) reconstitute with Ga^{3+}, giving rise to spectroscopically similar reconstitution products. EXAFS data obtained for both wild-type and mutant GaPdx are consistent with S_4 gallium ligation in both cases, although some differences in fine structure suggest that the side chain of residue 85 may be involved in second-shell interactions with the metal center (T. Barnhart and J. Penner-

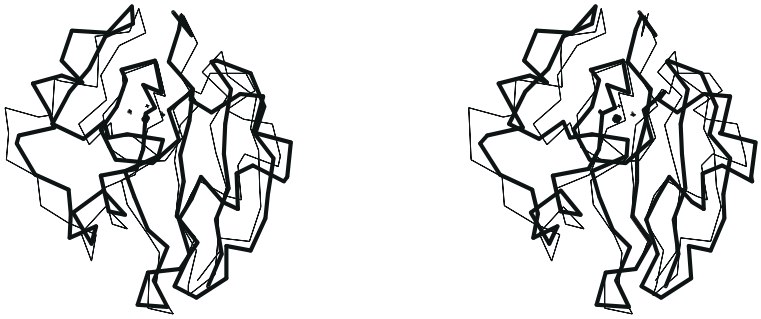

Fig. 6. Stereoview of the overlay of the C^{α} backbone trace of the NMR-derived model for the structure of native oxidized Pdx (Pochapsky et al., 1994a) and the global fold of GaPdx. The GaPdx fold is shown in heavy lines, and the native structure is shown in finer lines. The G helix, which shows the greatest difference between the two structures, is at the upper left of each view.

Hahn, unpublished results). NOEs identified between resonances in the metal binding site of GaPdx are completely consistent with this picture. Despite some overlap between the $C^{\beta}H_2$ proton resonance of the four cysteinyl ligands of the metal (Cys^{39}, Cys^{45}, Cys^{48} and Cys^{86}), it is possible to distinguish NOEs between the $C^{\beta}H_2$ protons of Cys^{39} and Cys^{86}, as well as NOEs between the $C^{\beta}H_2$ protons of Cys^{45} and Cys^{48}. A correlation between the NH resonance of Cys^{86} and the $C^{\beta}H$ protons of Cys^{48} is seen, confirming their proximity. Both the $C^{\alpha}H$ and $C^{\beta}H_2$ protons of Cys^{86} give rise to NOEs at the $C^{\beta}H_2$ protons of Met^{24}. The $C^{\beta}H_2$ protons of Cys^{39} give rise to NOEs at the $C^{\beta}H_3$ resonance of Ala^{43}, as well as at both methyl resonances of Leu^{84}. One methyl group of Leu^{84} also gives rise to NOEs at the $C^{\beta}H_2$ protons of Cys^{48}. The $C^{\varepsilon}H_3$ of Met^{70} shows NOEs to the $C^{\beta}H_2$ protons of Cys^{39} and Cys^{86}, the $C^{\alpha}H$ of Ser^{44} and both methyls of Leu^{84}. The $C^{\beta}H_2$ protons of Cys^{86} also show cross-relaxation with the $C^{\varepsilon}H_3$ of Met^{24}, indicating that both the Met^{24} and Met^{70} thioether groups are in close proximity to the metal binding site, and may provide some second-sphere interactions with the metal center. Although the $C^{\beta}H_2$ protons of Cys^{45} are somewhat broadened, a cross-cluster NOE is observed between the $C^{\beta}H_2$ protons of Cys^{45} and one of the $C^{\beta}H_2$ protons of Asp^{38}. A relatively long ^{15}N T_1 and a smaller than average $^{15}N\{^1H\}$ NOE for Cys^{45} suggest that this residue has more mobility than the other cysteinyl ligands of the metal center.

Other NOEs have been detected between resonances previously identified in native Pdx and others which can only be observed in the diamagnetic GaPdx. The most important of these involve the side chains of Tyr^{33} and Tyr^{51}. In NOESY spectra of native Pdx, only intraresidue and sequential NOEs were observed to the aromatic ring protons of Tyr^{33}. Unconstrained in structural calculations, the aromatic side chain of Tyr^{33} projected from the surface of the protein. In GaPdx, however, NOEs are observed from several residues to the aromatic protons of Tyr^{33}, including many of the side-chain protons of newly identified Met^{24} and the $C^{\alpha}H$ proton of Ser^{85}. These NOEs indicate that the ring of Tyr^{33} is partially imbedded in the surface of the protein, and plays a larger structural role than suggested by our model for the structure of the native protein (Pochapsky et al., 1994a). Since the chemical shifts of the Tyr^{33} ring protons do not differ significantly from those observed in native Pdx, it is likely that these interactions are not artifacts of gallium reconstitution, but are also present in the native protein.

Another new NOE is observed between one of the side-chain methyl groups of Leu^{71} and the ring protons of Tyr^{51}. The latter residue plays an important structural role in the formation of the C-terminal cluster of Pdx and, based on NOE data, this role is conserved in GaPdx. The new Leu^{71}–Tyr^{51} NOE suggests that the G helix may have a somewhat different tilt relative to the rest of the structure than is shown in our previous structural model. Helix G, although well defined as a structural feature, showed considerable mobility in previous structure calculations (Pochapsky et al., 1994a). We noted that this mobility was likely an artifact of the calculations, since few NOEs were available to restrain the G helix relative to the rest of the protein due to paramagnetic broadening. Met^{70} provides further restraints for the position of the G helix relative to the rest of the protein. NOEs are observed between the S-$C^{\varepsilon}H_3$ protons of Met^{70} and the methyls of Leu^{84}, the side chain of which abuts the metal binding site. An NOE is also observed from the Met^{70} S-$C^{\varepsilon}H_3$ resonance to the $C^{\alpha}H$ of Ser^{44} in the metal binding loop, providing information on close contacts between three different sections of the polypeptide chain. Figure 6 shows a superposition of the C^{α} trace of the published structure of native oxidized Pdx with that of GaPdx, indicating how the position of the G helix is shifted by the new NOE restraints.

Conclusions

The current work provides the first direct structural information regarding the metal binding site of a class of $Cys_4Fe_2S_2$ ferredoxins which are structurally, electronically and functionally distinct from those ferredoxins from cyanobacteria for which crystal structures have been

determined, such as *Anabaena* ferredoxin (Rypniewski et al., 1991). We are currently accumulating further structural constraints (stereospecific NOE assignments and dihedral angle constraints) in order to generate a high-resolution solution structure of GaPdx. This work is being done in conjunction with similar efforts for native Pdx, and it is expected that the GaPdx structure will provide a starting point for modeling the metal binding site in the native protein. We also expect that the GaPdx structure will be useful for molecular replacement analysis of X-ray diffraction data sets obtained for crystals of native Pdx (T. Arakaki, unpublished results).

Acknowledgements

This work was supported in part by a grant from the U.S. National Institutes of Health (GM-44191, T.C.P.). We thank Dr. Chris Arico-Muendel for help in setting up the multidimensional NMR experiments on the AMX-500, and Jill A. Walker, an undergraduate researcher from the University of Maryland Baltimore County who was supported by the Howard Hughes Summer Research Program, for access to her data on the treatment of GaPdx with iron salts. We thank Prof. James Penner-Hahn for access to EXAFS data collected on wild-type and mutant GaPdx. We gratefully acknowledge the generosity of Bruker Instruments Inc. in allowing access to spectrometers, and Susan Sondej Pochapsky and Clemens Anklin (Bruker Instruments, Billerica, MA, U.S.A.) for their advice and helpful discussions. T.C.P. acknowledges support from the U.S. National Science Foundation Young Investigator (CHE-9257036) and the Camille and Henry Dreyfus Teacher Scholars programs. S.K. acknowledges financial support from the NSERC (Canada) and FCAR (Quebec) graduate fellowship programs.

References

Anni, H., Vanderskooi, J.M. and Mayne, L. (1995) *Biochemistry*, **34**, 5744–5753.

Bax, A. and Davis, D.G. (1985) *J. Magn. Reson.*, **65**, 355–360.

Bax, A. and Subramanian, S. (1986) *J. Magn. Reson.*, **67**, 565–569.

Bax, A., Clore, G.M. and Gronenborn, A.M. (1990) *J. Magn. Reson.*, **88**, 425–431.

Bax, A. and Pochapsky, S.S. (1992) *J. Magn. Reson.*, **99**, 638–643.

Berg, A., Gustafsson, J.-Å., Ingelman-Sundberg, M. and Carlstrom, K. (1976) *J. Biol. Chem.*, **251**, 2831–2838.

Blake, P.R., Park, J.B., Zhou, Z.H., Hare, D.R., Adams, M.W.W. and Summers, M.F. (1992a) *Protein Sci.*, **1**, 1508–1521.

Blake, P.R., Day, M.W., Hsu, B.T., Joshua-Tor, L., Park, J.B., Hare, D.R., Adams, M.W.W., Rees, D.C. and Summers, M.F. (1992b) *Protein Sci.*, **1**, 1522–1525.

Clore, G.M., Driscoll, P.C., Wingfield, P.T. and Gronenborn, A.M. (1990) *Biochemistry*, **29**, 7387–7401.

Dugad, L.B. and La Mar, G.N. (1990) *Biochemistry*, **29**, 2263–2271.

Gerber, N.C., Horiuchi, T., Koga, H. and Sligar, S.G. (1990) *Biochem. Biophys. Res. Commun.*, **169**, 1016–1020.

Grzesiek, S. and Bax, A. (1992) *J. Magn. Reson.*, **96**, 432–440.

Grzesiek, S. and Bax, A. (1993) *J. Am. Chem. Soc.*, **115**, 12593–12594.

Kay, L.E., Torchia, D.A. and Bax, A. (1989) *Biochemistry*, **28**, 8972–8979.

Kay, L.E., Ikura, M., Tschudin, R. and Bax, A. (1990) *J. Magn. Reson.*, **89**, 496–514.

Kay, L.E., Xu, G.Y. and Yamazaki, T. (1994) *J. Magn. Reson.*, **A109**, 129–133.

Kazanis, S., Pochapsky, T.C., Barnhart, T.M., Penner-Hahn, J.E., Mirza, U.A. and Chait, B.T. (1995) *J. Am. Chem. Soc.*, **117**, 6625–6626.

Kraulis, P.J. (1991) *J. Appl. Crystallogr.*, **24**, 946–950.

Kumar, A., Ernst, R.R. and Wüthrich, K. (1980) *Biochem. Biophys. Res. Commun.*, **95**, 1–6.

Lippens, G., Dhalluin, C. and Wieruszeski, J.-M. (1995) *J. Biomol. NMR*, **5**, 327–331.

Lipscomb, J.D., Sligar, S.G., Namvedt, M.J. and Gunsalus, I.C. (1976) *J. Biol. Chem.*, **251**, 1116–1124.

Live, D.H., Davis, D.G., Agosta, W.C. and Cowburn, D. (1984) *J. Am. Chem. Soc.*, **106**, 1939–1941.

Lyons, T.A., Ratnaswamy, G. and Pochapsky, T.C. (1996) *Protein Sci.*, **5**, 627–639.

Majumdar, A. and Zuiderweg, E.R.P. (1993) *J. Magn. Reson.*, **B102**, 242–244.

Marion, D., Kay, L.E., Sparks, S.W., Torchia, D.A. and Bax, A. (1989a) *J. Am. Chem. Soc.*, **111**, 1515–1517.

Marion, D., Driscoll, P.C., Kay, L.E., Wingfield, P.T., Bax, A., Gronenborn, A.M. and Clore, G.M. (1989b) *Biochemistry*, **28**, 6150–6156.

McCoy, M.A. and Mueller, L. (1992a) *J. Am. Chem. Soc.*, **114**, 2108–2112.

McCoy, M.A. and Mueller, L. (1992b) *J. Magn. Reson.*, **98**, 674–679.

Neri, D., Otting, G. and Wüthrich, K. (1990) *J. Am. Chem. Soc.*, **112**, 3663–3665.

Olejniczak, E.T. and Eaton, H.L. (1990) *J. Magn. Reson.*, **87**, 628–632.

Piotto, M., Saudek, V. and Sklenář, V. (1992) *J. Biomol. NMR*, **2**, 661–665.

Pochapsky, T.C., Ye, X.M., Ratnaswamy, G. and Lyons, T.A. (1994a) *Biochemistry*, **33**, 6424–6432.

Pochapsky, T.C., Ratnaswamy, G. and Patera, A. (1994b) *Biochemistry*, **33**, 6433–6441.

Powers, R., Clore, G.M., Stahl, S.J., Wingfield, P.T. and Gronenborn, A. (1992) *Biochemistry*, **31**, 9150–9167.

Ratnaswamy, G. and Pochapsky, T.C. (1993) *Magn. Reson. Chem.*, **31**, S73–S77.

Rypniewski, W.R., Breiter, D.R., Benning, M.W., Wesenberg, G., Oh, B.-H., Markley, J.L., Rayment, I. and Holden, H.M. (1991) *Biochemistry*, **30**, 4126–4131.

Shaka, A.J., Keeler, J., Frenkiel, T. and Freeman, R. (1983) *J. Magn. Reson.*, **52**, 335–338.

Shaka, A.J., Barker, P.B. and Freeman, R. (1985) *J. Magn. Reson.*, **64**, 547–552.

Shaka, A.J., Lee, C.J. and Pines, A. (1988) *J. Magn. Reson.*, **77**, 274–293.

Skjeldal, L., Westler, W.M. and Markley, J.L. (1990) *Arch. Biochem. Biophys.*, **278**, 482–485.

Tanaka, M., Haniu, M., Yasunobu, K.T. and Kimura, T. (1973) *J. Biol. Chem.*, **248**, 1141–1157.

Ullah, A.H., Bhattacharyya, P.K., Bakthavachalam, J., Wagner, G.C. and Gunsalus, I.C. (1983) *Fed. Proc.*, **42**, 1897.

Van Zijl, P.C.M., Johnson, M.O., Mori, S. and Hurd, R.E. (1995) *J. Magn. Reson.*, **A113**, 265–270.

Vuister, G.W. and Bax, A. (1992) *J. Magn. Reson.*, **98**, 428–433.

Ye, X.M., Pochapsky, T.C. and Pochapsky, S.S. (1992) *Biochemistry*, **31**, 1961–1968.